Realization of rectangular fillet weld tracking based on rotating arc sensors and analysis of experimental results in gas metal arc welding

Jian Le[1, 2], Hua Zhang[1], XiaoQi Chen[2]
[1] Nanchang University, Key Laboratory of Robot &Welding Automation of Jiangxi, Nanchang 330031, PR China
[2] University of Canterbury, Department of Mechanical Engineering, Christchurch 8140, New Zealand

Abstract: In order to improve the welding quality and efficiency of the rectangular fillet weld in the shipyard and the steel structure workshop, reduce the labor cost, and improve the welding automation, it is necessary to study a welding robot that can track rectangular fillet weld. The working principle of the rotating arc sensor has been studied, and the mathematical model of the space posture of the arc welding gun has been established. The equivalent link coordinate systems of the wheeled mobile robot have been built, and the jacobian matrix of the robot and its inverse matrix have been calculated. The transformation from the operational space speed to the joint space speed has been realized by using the inverse matrix of the jacobian matrix, and the trajectory planning of the welding robot has been finished. The tracking algorithms of the linear fillet weld and the rectangular fillet weld have been studied, and the rectangular fillet weld tracking experiment has been done in the laboratory and the factory. Experimental results showed that the welding robot can track the rectangular fillet weld with high accuracy and good reliability.

Keywords: Rotating arc sensors; Robot; Kinematics analysis; Rectangular fillet weld tracking; Experimental data analysis

1 Introduction

Welding is one of the most effective ways of metal connection, the cost is low, and the connection is reliable. In the steel structure workshop and the shipbuilding industry, there are a large number of rectangular fillet welds. The automatic welding carriage can weld the straight welding seam, and the welding point locates in the line that passes through two points where two guide wheels contact the vertical steel plate of fillet weld. When the welding seam is curve, the welding point deviates from the welding seam, so the automatic welding carriage cannot weld the rectangular fillet weld. The size of the mechanical arm is big, and it is not convenient to move, so it cannot weld the rectangular fillet weld in a narrow place. Therefore, the rectangular fillet weld is welded by the manual welding. During the welding process, there are arc light, splash, and toxic gas. The working environment is very bad, which makes that the workers are easy to suffer from all kinds of diseases, and the welding quality is poor. In addition, the welding efficiency is low, and the cost is high, so it is necessary to research a kind of welding robot that can track the rectangular fillet weld.

There are electromagnetic fields, strong arc light, spatter, and smoke during the welding process, so many sensors cannot work normally, but the visual and arc sensors are widely used in tracking the welding seam. Ku et al. [1] studied development of a mobile welding robot for double-hull structures in shipbuilding. Liu et al. [2] designed robot welding seam tracking system with structured light vision. Nele et al. [3] established an image acquisition system for real-time seam tracking. Gu et al. [4] analyzed autonomous seam acquisition and tracking system for multi-pass welding based on vision sensor. Xu et al. [5] established computer vision technology for seam tracking in robotic GTAW and GMAW, a set of special vision system had been designed, which could acquire clear and steady real-time weld images, and results showed that the precision of this vision based tracking technology was very high. Chen and Feng [6] studied the model of underwater wet welding process based on visual and arc sensors. Xu et al. [7] developed real-time seam tracking control technology during welding robot GTAW process based on passive vision sensors, a segmented self-adaptive PID controller was introduced, and experiments showed that the seam tracking accuracy could meet the requirements of quality control of seam forming. Shen et al. [8] proposed real-time seam tracking technology of welding robot with visual sensing. Xu et al. [9] studied the real-time tracking information of three-dimension welding seam in robotic GTAW process based on composite sensor technology, the paper designed a set of composite sensor system, which could acquire three-dimensional welding seam information, and the results demonstrate that the error was very small, which was accurate enough to meet the requirement of the real-time tracking and controlling. Wang [10] proposed three-dimensional vision-based sensing of GTAW a review. Because of the influence of the strong arc light and smoke, there are a lot of noises in the images when the welding seam is identified by using the visual sensor, so the filtering algorithm, the deviation identification algorithm and the control algorithm are complex. In addition, the amount of calculation of the image processing is big, so it is not conducive to the real-time tracking of the welding seam. When the arc sensor is used in tracking the welding seam, the welding point is the detecting point, the real-time performance is strong, and it is not influenced by arc light, spatter and smoke, so it is widely used in the tracking system of the fillet weld. Kim and Na [11] studied an arc sensor model for gas metal arc welding with rotating arc about dynamic simulation of wire melting, and it was clarified how the characteristics of the welding power source affected the sensitivity of the arc sensor. Kim and Na [12] studied an arc sensor model for gas metal arc welding with rotating arc about simulation of an arc sensor in mechanically rotating gas metal arc welding, and a mathematical model for the dynamic behaviour of the electrode melting rate and arc length was presented. Lee et al. [13] developed a high speed rotating arc sensor system for tracking complicate curved fillet welding lines. Kim and Rhee [14] designed the arc sensor model by using multiple-regression analysis and a neural network, and different types of regression models were developed. Yoo et al. [15] proposed end point detection of fillet weld using the mechanized rotating arc sensor in GMAW, and a geometrical sensing model was developed. Shi et al. [16] studied the mathematical model of the rotational arc sensor in GMAW and its applications to seam tracking and endpoint detection, and the mathematical model could be

helpful for the interpretation and improvement of arc sensing systems. Xu et al. [17] researched the acquisition and processing of real-time information for height tracking of robotic GTAW process by arc sensors, this paper designed a set of arc sensor system for height tracking of weld seam, which was accurate enough to meet the requirements of the height tracking and controlling, and the experimental results showed that the height error between the calculated arc length and the real arc length was very small.

The size of the rectangular fillet weld is not constant in the factory, the working space is narrow, and one rectangular fillet weld has four right-angle fillet welds, so it is difficult to track the rectangular fillet weld. In recent years, research of the rectangular fillet weld tracking in a narrow space is fewer. In order to reduce the welding cost, and improve the welding quality and efficiency, it is necessary to research a kind of autonomous mobile welding robot, and it can track rectangular fillet welds of various sizes, so some economic and social benefits can be generated by using this robot.

2 The mathematical model of the rectangular fillet weld

Fig. 1 shows some rectangular fillet welds in the steel structure workshop and the mathematical model of the rectangular fillet weld. and Fig. 1(a) shows that the steel beam consists of many rectangular fillet welds. In order to improve the strength of the steel beam and the ability to resist bending, and reduce the weight of the steel beam, the cross section of the steel beam is usually the H shape. During the manufacturing process of the steel beam of the H shape, many rectangular fillet welds need to be welded. Fig. 1(b) shows the real figure of two rectangular fillet welds, four sides of the rectangular fillet weld are short, and the working space is very small, so the welding quality and efficiency will be affected.

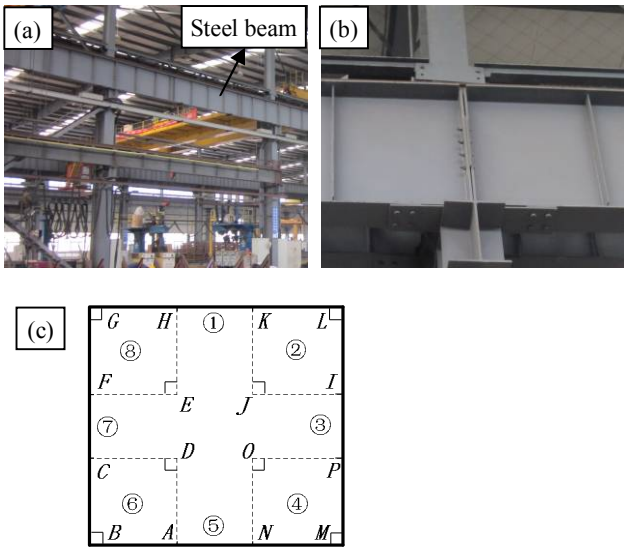

Fig. 1 Some rectangular fillet welds in the steel structure workshop and the mathematical model of the rectangular fillet weld. (a) the steel beam consists of many rectangular fillet welds; (b) the real figure of two rectangular fillet welds; (c) the mathematical model of the rectangular fillet weld

Fig. 1(c) shows the mathematical model of the rectangular fillet weld, and a rectangular fillet weld consists of four right-angle fillet welds(②, ④, ⑥, ⑧) and four linear fillet welds(①, ③, ⑤, ⑦). Because of the assembly error, the angle of the right-angle fillet weld is not 90°, and it is a value between 80° and 100°. Because of the deformation of the steel plates, the fillet weld is not a straight line, and it is the space curve fillet weld actually. If the linear fillet weld and the right-angle fillet weld can be tracked by the welding robot, the rectangular fillet weld tracking will be realized.

Many steel structure factories use the automatic welding carriage to weld the straight-line welding seam, but it cannot weld the space curve fillet weld and the right-angle fillet weld well. The steel beam is big, and it is not convenient to be moved. In addition, the size of the mechanical arm is big, and it also cannot move independently, so the mechanical arm cannot be applied in welding the rectangular fillet weld in the steel beam. At present, the rectangular fillet welds are mainly welded by the manual welding. In order to improve the welding quality and efficiency, and enhance the welding automation, it is necessary to research a kind of welding robot with light weight and small size.

3 The structure of the robot and the whole system of fillet weld tracking and welding

In order to make a clear introduction of the internal structure of the robot in Fig. 2, the shell of the welding robot has been removed. Fig. 2(a) is the real figure, and Fig. 2(b) is the schematic diagram.

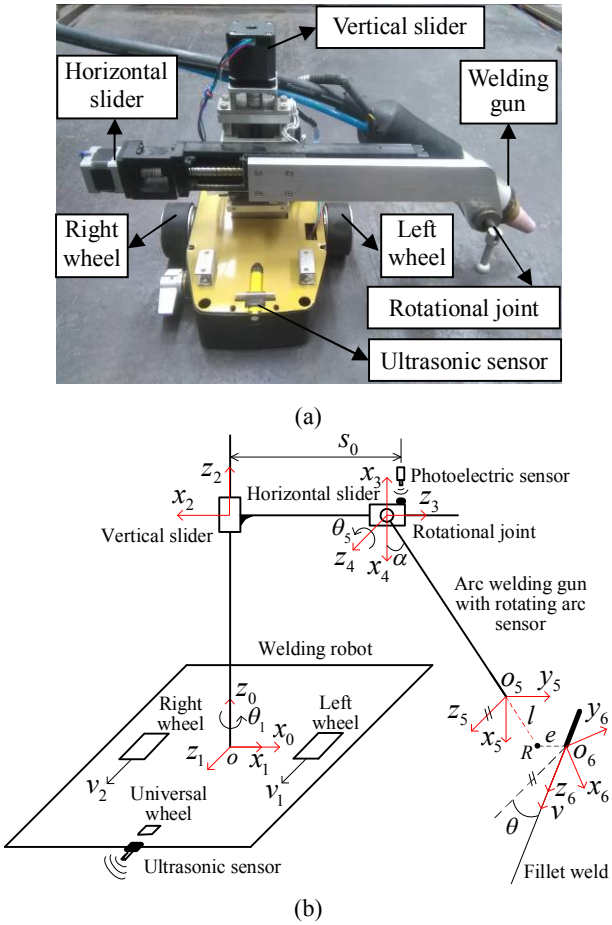

Fig. 2 The robot. (a) The real figure; (b) The schematic diagram

The welding robot is made up of the left and right wheels, the vertical slider, the horizontal slider, the

rotational joint, the arc welding gun with rotating arc sensor, the ultrasonic sensor, the photoelectric position sensor and the universal wheel. The ultrasonic sensor can measure the distance between the front of the robot and the front steel plate, and it is the linear relationship between the distance and the voltage of the output. The larger the distance is, the greater the voltage of the output will be. When the distance is equal to the set value, the robot begins to track the right-angle fillet weld. The photoelectric position sensor consists of the photoelectric switch and the reflector plate, and the photoelectric switch can send and receive light. The reflector plate is fixed to the horizontal slider, and it will also move when the horizontal slider moves. When the horizontal slider is in the initial position, the photoelectric switch can receive the light reflected by the reflector plate, and the photoelectric position sensor will output a signal. Extension or indentation of the horizontal slider can be identified by using the photoelectric position sensor and the movement speed of the horizontal slider. Rectangular fillet weld tracking can be realized based on the coordinated movement among two wheels, the horizontal slider and the vertical slider. In Fig. 2(b), the equivalent link coordinate systems of the wheeled mobile robot have been built, and the principle of each coordinate system will be introduced in Section 5.1.

Fig. 3 is the whole system of tracking and welding during gas metal arc welding process, and the whole system includes the welding system and the welding seam tracking system. The welding system mainly includes the welding power source, the wire feeder, shielding gas, one cable and one workpiece. The positive electrode of the welding power source connects with the welding wire, and the negative electrode of the welding power source connects with the workpiece. At the same time, the control signal in the signal line can control the wire feeding speed, which makes the wire feeding speed match the current welding current and voltage, so the arc is stable. In order to prevent the welding area from oxidizing, the welding area should be protected by shielding gas during the welding process. The welding seam tracking system mainly includes the mechanical parts, rotating arc sensor, ultrasonic sensors, hall sensor, photoelectric position switch, power source, motor driver, the movement control card ART1020, the industrial control computer PCM3343, the data acquisition card ART2932, the measurement and control circuit board of arc rotating speed, human-computer interaction interface, and the control and display circuit board of the working state. The mechanical parts of the robot have been introduced in Fig. 2, so we are not going to introduce the mechanical parts again. By using the single chip microcomputer system in the measurement and control circuit board of arc rotating speed, arc rotating speed can be measured and controlled, so the arc rotating speed is approximately 25 HZ, and the circuit board sends the position signal of arc to the industrial control computer. According to the results of program execution in the industrial control computer, striking or extinguishing arc can be controlled by using the measurement and control circuit board of arc rotating speed. The data acquisition card can collect the welding currents by using the hall sensor, and the space posture of the arc welding gun can be recognized by analyzing the waveform of the welding currents. The data acquisition card collects the output data of the ultrasonic sensor, and the straight-line distance between the front of the robot and the front obstacle can be obtained.

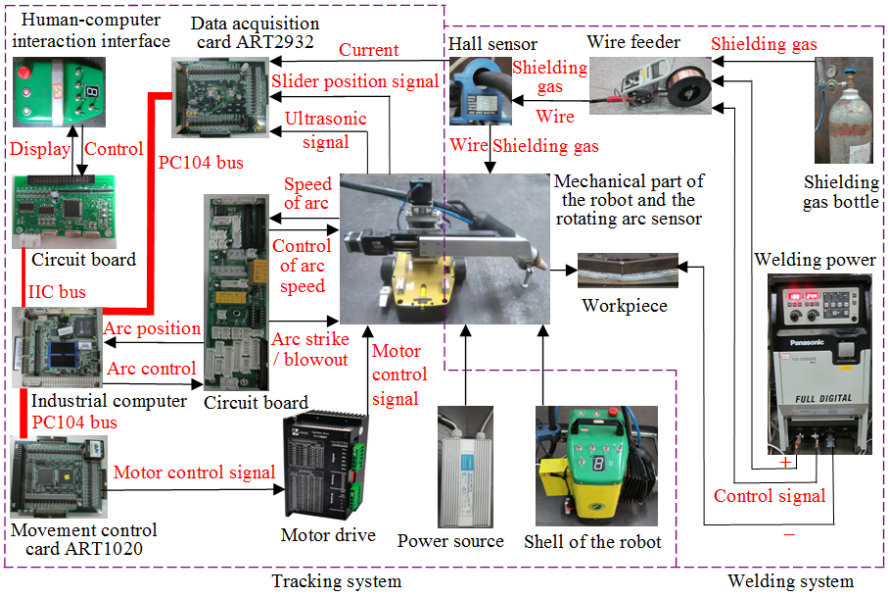

Fig. 3 The whole system of tracking and welding

By using the photoelectric position switch, the data acquisition card can collect the position signal of the horizontal slider and the vertical slider. By using the PC104 bus, the industrial control computer sets the sampling frequency and other parameters of the data acquisition card, and collects the signals from the data acquisition card. By running the execution program in the industrial control computer, signal filtering, deviation identification and the control algorithm can be finished, and the calculation results of the control algorithm can be used to control the movement of the sliders and two wheels by using the movement control card and the motor drives, so the welding seam tracking can be realized. In order to improve the reliability and the operability of the robot, the control and display circuit board of the working state has been designed, and workers can observe and

control the state of the robot in real time by manipulating the buttons and observing the display on the human-computer interaction interface. At the same time, the voltage source is required, and it can convert the voltage from 220 V to 24 V. In order to improve the reliability of the welding robot in the factory environment, the metal shell is required to protect some electronic parts. Finally, the introduction for the whole system of tracking and welding has been completed.

4 Working principle of rotating arc sensor and the mathematical model of space posture of the welding gun

Fig. 4 shows the working principle of the rotating arc sensor, and the arc welding gun deviates from fillet weld to the right and tilts forward along the welding direction. The rotating arc sensor with the welding wire rotates counterclockwise, and the angular velocity is w. At the same time, the welding arc rotates at the same angular velocity, and the rotational radius is r. The arc welding gun goes through position 1, 2, 3, 4, and 1 in turns, and the equivalent wire extension is the length of the line segment DD'' when the welding arc rotates one circle. The relationship between the wire extension and the welding current is linear, and the mathematical model of their relationship can be established. When the welding arc rotates one circle, an average value corresponding to welding currents can be computed, so the equivalent wire extension l can be identified by using the mathematical model between the wire extension and the welding current. In order to avoid repetition, the recognition algorithm of the equivalent wire extension can refer to Reference [18].

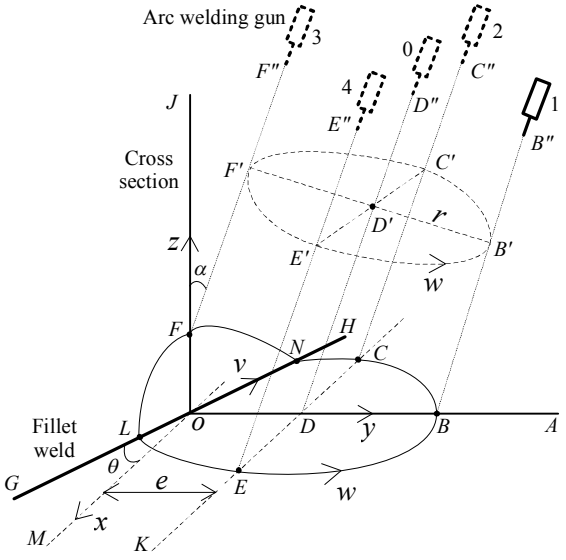

Fig. 4 The arc welding gun deviates from fillet weld to the right and tilts forward

The linear fillet weld can be divided into many short fillet welds, and every short fillet weld is approximate to a straight line. The current welding point is regarded as the origin point of the coordinate system, and the vertical direction is regarded as z axis. The projection of the equivalent wire extension is regarded as y axis in the horizontal plane, and the direction of x axis can be determined according to the right-hand rule, so the coordinate system $oxyz$ has been established. Point D is the intersection point between the equivalent wire extension DD'' and the horizontal plane oxy, and x axis is parallel to the line CE that passes the point D. The distance between x axis and the line CE is regarded as the horizontal deviation that the arc welding gun deviates from fillet weld. When the coordinate of the point D on the y axis is positive, the arc welding gun deviates from fillet weld to the right along the welding direction; When the coordinate of the point D on the y axis is negative, the arc welding gun deviates from fillet weld to the left along the welding direction. Line GH is fillet weld, and the welding speed is v. When the wire extension is within a certain range, the longer the wire extension is, the smaller the welding current will be. When the welding arc rotates from point B to point N counterclockwise, the wire extension turns longer, and the welding current turns smaller; When the welding arc rotates from point N to point F counterclockwise, the wire extension turns shorter, and the welding current turns larger; When the welding arc rotates from point F to point L and point B counterclockwise, the wire extension turns longer, then shorter, so the welding current turns smaller, then larger. When the welding arc rotates one circle, 64 welding currents are collected by the hall sensor. If the sum of welding currents corresponding to the curve EBC is bigger than the sum of welding currents corresponding to the curve $CNFLE$, the horizontal deviation e is greater than zero, and the arc welding gun deviates from fillet weld to the right along the welding direction. Otherwise, the horizontal deviation e is smaller than zero when it is not zero, and the arc welding gun deviates from fillet weld to the left along the welding direction. The horizontal deviation e can be computed,

$$e=\begin{cases}\dfrac{-r\Delta I}{\Delta I_{\max l}} & \Delta I \le 0\\[2ex] \dfrac{r\Delta I}{\Delta I_{\max r}} & \Delta I > 0\end{cases} \tag{1}$$

Where ΔI is the difference that the sum of welding currents corresponding to the curve EBC subtracts the sum of welding currents corresponding to the curve $CNFLE$, r is the rotational radius of the welding arc, and e is the horizontal deviation that the arc welding gun deviates from fillet weld. When the arc welding gun deviates from fillet weld to the left along the welding direction, the difference ΔI and the horizontal deviation e are less than zero, and $\Delta I_{\max l}$ is the smallest value of ΔI, but the absolute value of $\Delta I_{\max l}$ is the largest. When the arc welding gun deviates from fillet weld to the right along the welding direction, the difference ΔI and the horizontal deviation e are bigger than zero, and $\Delta I_{\max r}$ is the biggest value of ΔI. When the horizontal distance that the arc welding gun deviates from fillet weld is bigger than the rotational radius r of the welding arc, the absolute value of the horizontal deviation e is biggest, and its value is equal to r.

The angle between the equivalent wire extension DD'' and z axis is the inclination angle α of the arc welding gun in the vertical plane, and the inclination angle α can be changed by the rotational joint of the welding robot. When the inclination angle α is $45°$ during the flat welding process, the welding arc is stable, so the inclination angle α of the arc welding gun in the vertical plane is $45°$ in this paper. The angle between the fillet weld GH and x axis is the size of the inclination angle θ of the arc welding gun along the welding direction. When fillet weld GH is in the second and fourth quadrants of the coordinate system oxy, the inclination angle θ of the arc welding gun is bigger than $0°$, and the arc welding gun tilts forward along the welding direction; When fillet weld GH is in the first and third quadrants of the coordinate system oxy, the inclination angle θ of the arc welding gun is smaller than $0°$, and the arc welding gun tilts backward along the welding direction. Fig. 5 shows the calculating algorithm of the inclination angle θ of the arc welding gun along the welding direction, Fig. 5(a) shows that the arc welding gun tilts backward along the welding direction and θ is smaller than $0°$, and Fig. 5(b) shows that the arc welding gun tilts forward along the welding direction and θ is bigger than $0°$.

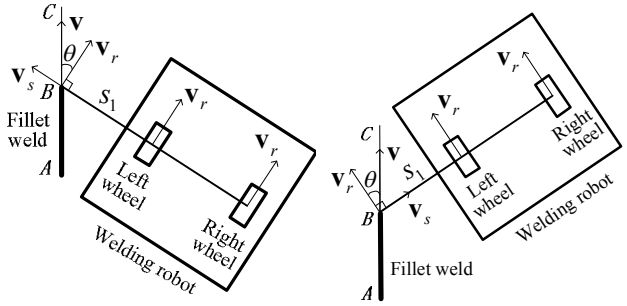

Fig. 5 Inclination angle of the arc welding gun along the welding direction. (a) The arc welding gun tilts backward along the welding direction; (b) The arc welding gun tilts forward along the welding direction

In Fig. 5, the speed of the left wheel is equal to the speed of the right wheel, so the trajectory of the center point of the robot is a line, and the robot tracks the fillet weld based on movement of the horizontal slider. When the horizontal slider extends, the speed v_s of the horizontal slider is less than zero; When the horizontal slider indents, the speed v_s of the horizontal slider is bigger than zero. The inclination angle θ of the arc welding gun along the welding direction can be computed by the following equation,

$$\theta = \arctan(\frac{v_s t}{v_r t}) = \arctan(\frac{v_s}{v_r}) \tag{2}$$

Where θ is the inclination angle of the arc welding gun along the welding direction, v_r is the speed of the robot, v_s is the speed of the horizontal slider, and t is the time when the inclination angle θ is identified.

Identification of the space posture of the arc welding gun has been researched based on the rotating arc sensor, and the mathematical model of the space posture of the arc welding gun can be expressed as $\mathbf{P} = (l, e, \alpha, \theta)$. $\mathbf{P}$ is a vector that represents the space posture of the arc welding gun, l is the equivalent wire extension, e is the horizontal deviation, α is the inclination angle of the arc welding gun in the vertical plane, and θ is the inclination angle of the arc welding gun along the welding direction. The deviations of the space posture of the arc welding gun can be computed by comparing the current space posture with the target space posture, so the welding robot can track the linear fillet weld in the rectangular fillet weld based on the coordinated movement among two wheels, the horizontal slider and the vertical slider.

5 Research on the kinematics of the welding robot

5.1 Establishing the equivalent link coordinate systems of the wheeled mobile robot

Fig. 6 shows that the welding robot rotates counterclockwise, the arc DCE is the trajectory of endpoint of the welding wire. and r_1 is radius of the arc DCE. v is the welding speed, w_1 is the rotating angular velocity of the robot. a_1 is the distance between the current welding point C and the center point B of the left wheel, b_1 is the distance between the center point A of the right wheel and the center point B of the left wheel, v_1 is the speed of the left wheel, v_2 is the speed of the right wheel. As shown in Fig. 6(a), the kinematics of the robot is studied in the coordinate system that its original point is the rotational center point of the robot, and the movement of the robot is the rotation around the center of the circle corresponding to the arc DCE. As shown in Fig. 6(b), the kinematics of the robot is studied in the coordinate system that its original point is the center point O of the robot, and the movement of the robot consists of the translational movement of the robot and the rotation around the center point O of the robot.

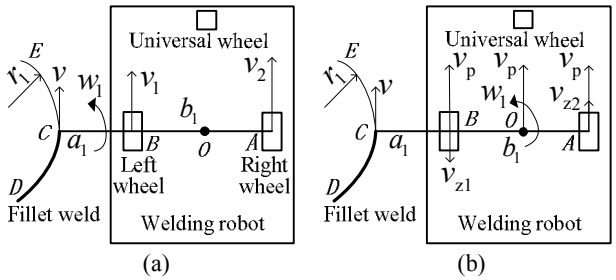

Fig. 6 The welding robot rotates counterclockwise. (a) the kinematics of the robot is studied in the coordinate system that its original point is the center of the circle corresponding to the arc DCE; (b) the kinematics of the robot is studied in the coordinate system that its original point is the center point O of the robot

The speed v_p of the translational movement of the robot in Fig. 6(b) is equal to the rotational speed of the center point O of the robot in Fig. 6(a), and it can be

computed by the following equation,

$$v_p = w_1(r_1 + a_1 + b_1/2) \tag{3}$$

When the welding robot rotates counterclockwise around the center point O of the robot, the angular velocity is w_1, so the rotational speed of the left wheel is v_{z1}, the rotational speed of the right wheel is v_{z2}, and they satisfy the following equation,

$$v_{z1} = v_{z2} = w_1 b_1/2 \tag{4}$$

The movement of the robot is the same in Fig. 6(a) and Fig. 6(b), but the same movement is described by two different coordinate systems, so the resultant speed v_1 of the left wheel can be computed by the following equation,

$$v_1 = v_p - v_{z1} = (r_1 + a_1)w_1 = (r_1 + a_1)\, v/r_1 \tag{5}$$

and the resultant speed v_2 of the right wheel can be computed by the following equation,

$$v_1 = v_p + v_{z2} = (r_1 + a_1 + b_1)w_1 = (r_1 + a_1 + b_1)\, v/r_1 \tag{6}$$

In equations (3-6), the meanings of the physical quantities have already been introduced in the front.

Fig. 7 shows that the welding robot rotates clockwise. As shown in Fig. 7(a), the kinematics of the robot is studied in the coordinate system that its original point is the center of the circle corresponding to the arc DCE. As shown in Fig. 7(b). the kinematics of the robot is studied in the coordinate system that its original point is the center point O of the robot, and the movement of the robot consists of the translational movement of the robot and the rotation around the center point O of the robot. The meanings of the physical quantities are the same as those in Fig. 6. When $r_1 > a_1 + b_1$, the robot moves smoothly, so this situation is discussed below,

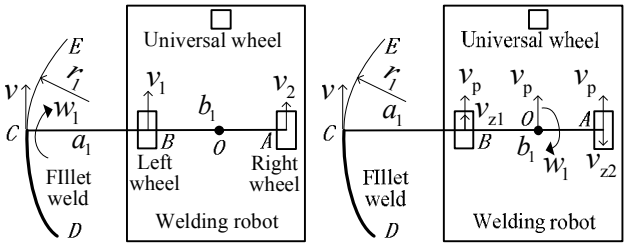

Fig. 7 The welding robot rotates clockwise. (a) the kinematics of the robot is studied in the coordinate system that its original point is the center of the circle corresponding to the arc DCE; (b) the kinematics of the robot is studied in the coordinate system that its original point is the center point O of the robot

The speed v_p of the translational movement of the robot in Fig. 7(b) is equal to the rotational speed of the center point O of the robot in Fig. 7(a), and it can be computed by the following equation,

$$v_p = w_1(r_1 - a_1 - b_1/2) \tag{7}$$

When the welding robot rotates clockwise around the center point O of the robot, the rotational speed v_{z1} of the left wheel and the rotational speed v_{z2} of the right wheel satisfy the following equation,

$$v_{z1} = v_{z2} = w_1 b_1/2 \tag{8}$$

The movement of the robot is the same in Fig. 7(a) and Fig. 7(b), but the same movement is described by two different coordinate systems, so the resultant speed v_1 of the left wheel can be computed by the following equation,

$$v_1 = v_p + v_{z1} = (r_1 - a_1)w_1 = (r_1 - a_1)\, v/r_1 \tag{9}$$

and the resultant speed v_2 of the right wheel can be computed by the following equation,

$$v_1 = v_p - v_{z2} = (r_1 - a_1 - b_1)w_1 = (r_1 - a_1 - b_1)\, v/r_1 \tag{10}$$

In equations (7-10), the meanings of the physical quantities are the same as those in equations (3-6).

As shown in Fig. 6 and Fig. 7, movement of two wheels of the wheeled mobile robot is equivalent to the translational movement and the rotational movement around the center point O of the robot, so two wheels of the wheeled mobile robot are equivalent to a translational joint and a rotational. By using the D-H parametric method that it has been studied in Reference [19], the coordinate systems of joints of the robot have been established in Fig. 2(b), and the equivalent link coordinate systems of the wheeled mobile robot have been established in Fig. 8.

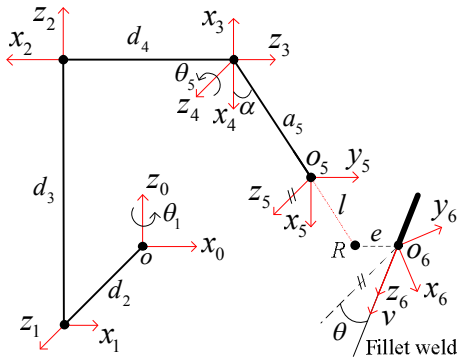

Fig. 8 The equivalent link coordinate systems of the wheeled mobile robot

As shown in Fig. 8, the coordinate system $ox_0y_0z_0$ is fixed to the rotational joint 1, and it is also the coordinate system of the link 1. At the same time, the base coordinate system is the same as the coordinate system $ox_0y_0z_0$. The coordinate system $o_1x_1y_1z_1$ is fixed to the translational joint 2, and it is also the coordinate system of the link 2; The coordinate system $o_2x_2y_2z_2$ is fixed to the translational joint 3, and it is also the coordinate system of the vertical slider; The coordinate system $o_3x_3y_3z_3$ is fixed to the translational joint 4, and it is also the coordinate system of the horizontal slider; The coordinate system $o_4x_4y_4z_4$ is fixed to the rotational

joint 5, and it is also the coordinate system of the link 5; The coordinate system $o_5x_5y_5z_5$ is fixed to endpoint of the contact tube, and it is also the tool frame; The coordinate system $o_6x_6y_6z_6$ is the target coordinate system that its original point is the current welding point on the welding seam.

In Fig. 8, l is the equivalent wire extension, e is the horizontal deviation, α is the inclination angle of the arc welding gun in the vertical plane, and θ is the inclination angle of the arc welding gun along the welding direction. θ_1 is the rotational angle around the rotating joint 1 , d_2 is the distance between the link 2 and the link 3, d_3 is the distance between the link 3 and the link 4, d_4 is the distance between the link 4 and the link 5, θ_5 is the rotational angle around the rotating joint 5, a_5 is the length of the arc welding gun, and v is the welding speed.

Table 1 shows the parameter list of the equivalent link in Fig. 8, α_{i-1} is the torsional angle of a link, a_{i-1} is the length of a link, d_i is the distance between the link i and the link $i+1$, θ_i is the included angle between the link i and the link $i+1$, and the meanings of other physical quantities are the same as those in Fig. 8.

Table 1 The parameter list of the equivalent link in Fig. 8

Link i	Variable	α_{i-1}	a_{i-1}	d_i	θ_i
1	θ_1	0°	0	0	θ_1
2	d_2	90°	0	d_2	180°
3	d_3	90°	0	d_3	–90°
4	d_4	90°	0	d_4	270°
5	θ_5	90°	0	0	θ_5

According to the Reference [19], the homogeneous transformation matrix ${}^{i-1}\mathbf{T}_i$ that the coordinate system of the link i is relative to the coordinate system of the link $i-1$ can be computed in the following equation,

$$ {}^{i-1}\mathbf{T}_i = \begin{bmatrix} \mathrm{c}\theta_i & -\mathrm{s}\theta_i & 0 & a_{i-1} \\ \mathrm{s}\theta_i\mathrm{c}\alpha_{i-1} & \mathrm{c}\theta_i\mathrm{c}\alpha_{i-1} & -\mathrm{s}\alpha_{i-1} & -d_i\mathrm{s}\alpha_{i-1} \\ \mathrm{s}\theta_i\mathrm{s}\alpha_{i-1} & \mathrm{c}\theta_i\mathrm{s}\alpha_{i-1} & \mathrm{c}\alpha_{i-1} & d_i\mathrm{c}\alpha_{i-1} \\ 0 & 0 & 0 & 1 \end{bmatrix} \quad (11) $$

Where c represents cos , s represents sin , and other physical quantities are the same as those in Table 1.

The parameters of each link in Table 1 are substituted in Equation (11), the homogeneous transformation matrix of each link can be computed in the following equation,

$$ {}^{0}\mathbf{T}_1(\theta_1) = \begin{bmatrix} \mathrm{c}\theta_1 & -\mathrm{s}\theta_1 & 0 & 0 \\ \mathrm{s}\theta_1 & \mathrm{c}\theta_1 & 0 & 0 \\ 0 & 0 & 1 & 0 \\ 0 & 0 & 0 & 1 \end{bmatrix} $$

$$ {}^{1}\mathbf{T}_2(d_2) = \begin{bmatrix} -1 & 0 & 0 & 0 \\ 0 & 0 & -1 & -d_2 \\ 0 & -1 & 0 & 0 \\ 0 & 0 & 0 & 1 \end{bmatrix} $$

$$ {}^{2}\mathbf{T}_3(d_3) = \begin{bmatrix} 0 & 1 & 0 & 0 \\ 0 & 0 & -1 & -d_3 \\ -1 & 0 & 0 & 0 \\ 0 & 0 & 0 & 1 \end{bmatrix} $$

$$ {}^{3}\mathbf{T}_4(d_4) = \begin{bmatrix} 0 & 1 & 0 & 0 \\ 0 & 0 & -1 & -d_4 \\ -1 & 0 & 0 & 0 \\ 0 & 0 & 0 & 1 \end{bmatrix} $$

$$ {}^{4}\mathbf{T}_5(\theta_5) = \begin{bmatrix} \mathrm{c}\theta_5 & -\mathrm{s}\theta_5 & 0 & 0 \\ 0 & 0 & -1 & 0 \\ \mathrm{s}\theta_5 & \mathrm{c}\theta_5 & 0 & 0 \\ 0 & 0 & 0 & 1 \end{bmatrix} \quad (12) $$

Where c represents cos , s represents sin , ${}^{0}\mathbf{T}_1(\theta_1)$ is the homogeneous transformation matrix that the coordinate system of the link 1 is relative to the base coordinate system, and ${}^{i-1}\mathbf{T}_i$ is the homogeneous transformation matrix that the coordinate system of the link i is relative to the coordinate system of the link $i-1$. Other physical quantities are the same as those in Table 1.

${}^{5}\mathbf{T}_6$ is the homogeneous transformation matrix that the tool frame $o_5x_5y_5z_5$ is relative to the coordinate system $o_4x_4y_4z_4$, the matrix can be computed in the following equation,

$$ {}^{5}\mathbf{T}_6 = \begin{bmatrix} 1 & 0 & 0 & \dfrac{\sqrt{2}a_5}{2} \\ 0 & 1 & 0 & \dfrac{\sqrt{2}a_5}{2} \\ 0 & 0 & 1 & 0 \\ 0 & 0 & 0 & 1 \end{bmatrix} \quad (13) $$

5.2 Calculating the jacobian matrix of the equivalent link system of the wheeled mobile robot and its inverse matrix

The homogeneous transformation matrix ${}^{i}\mathbf{T}_6$ that the tool frame $o_5x_5y_5z_5$ is relative to the coordinate system

of the link i can be computed by using the matrix ${}^{i-1}\mathbf{T}_i$ in Section 5.1, and it has been shown in the following equation,

$$ {}^{i}\mathbf{T}_6 = {}^{i}\mathbf{T}_{i+1} \bullet\bullet\bullet {}^{5}\mathbf{T}_6 \qquad i = 1,2,3,4,5 \tag{14} $$

Where ${}^{i}\mathbf{T}_{i+1}$ is the homogeneous transformation matrix that the coordinate system of the link $i+1$ is relative to the coordinate system of the link i, ${}^{i}\mathbf{T}_6$ is the homogeneous transformation matrix that the tool frame $o_5x_5y_5z_5$ is relative to the coordinate system of the link i.

According to the Reference [19], the jacobian matrix $\mathbf{J}$ of the robot can be computed by using the matrix ${}^{i}\mathbf{T}_6$, and the matrix shows the velocity ratio from the joint space to the operational space. The jacobian matrix $\mathbf{J}$ has been shown in the following equation,

$$ \mathbf{J} = \left[\begin{array}{c|c|c|c|c|c} 0 & d_2\,\mathrm{s}_5 & 0 & -\mathrm{c}_5 & \mathrm{s}_5 & 0 \\ 0 & d_2\,\mathrm{c}_5 & 0 & \mathrm{s}_5 & \mathrm{c}_5 & 0 \\ 0 & -\frac{\sqrt{2}}{2}a_5(\mathrm{s}_5+\mathrm{c}_5)-d_4 & 1 & 0 & 0 & 0 \\ 0 & -\mathrm{c}_5 & 0 & 0 & 0 & 0 \\ 1 & \mathrm{s}_5 & 0 & 0 & 0 & 0 \\ 0 & 0 & 0 & 0 & 0 & 1 \end{array}\right] \tag{15} $$

Where s_5 represents $\sin\theta_5$, c_5 represents $\cos\theta_5$, d_2 is the distance between the link 2 and the link 3, d_4 is the distance between the link 4 and the link 5, and a_5 is the length of the arc welding gun.

When the inclination angle α of the welding gun in the vertical plane is $45°$ during the flat welding process, the welding arc is stable, so the rotational angle θ_5 around the rotating joint 5 is $0°$. In addition, the distance d_2 between the link 2 and the link 3 is 0, so the jacobian matrix $\mathbf{J}_1$ during the flat welding process has been shown in the following equation,

$$ \mathbf{J}_1 = \left[\begin{array}{cccccc} 0 & 0 & 0 & -1 & 0 & 0 \\ 0 & 0 & 0 & 0 & 1 & 0 \\ 0 & -\frac{\sqrt{2}}{2}a_5 - d_4 & 1 & 0 & 0 & 0 \\ 0 & -1 & 0 & 0 & 0 & 0 \\ 1 & 0 & 0 & 0 & 0 & 0 \\ 0 & 0 & 0 & 0 & 0 & 1 \end{array}\right] \tag{16} $$

The inverse matrix $\mathbf{J}_1^{-1}$ of the jacobian matrix shows the velocity ratio from the operational space to the joint space, and it has been shown in the following equation,

$$ \mathbf{J}_1^{-1} = \left[\begin{array}{cccccc} 0 & 0 & 0 & 0 & 1 & 0 \\ 0 & 0 & 0 & -1 & 0 & 0 \\ 0 & 0 & 1 & -\frac{\sqrt{2}}{2}a_5 - d_4 & 0 & 0 \\ -1 & 0 & 0 & 0 & 0 & 0 \\ 0 & 1 & 0 & 0 & 0 & 0 \\ 0 & 0 & 0 & 0 & 0 & 1 \end{array}\right] \tag{17} $$

In equations (16-17), the meanings of the physical quantities are the same as those in Equation (15).

5.3 Calculating the joint speed of the equivalent link system

The inverse matrix $\mathbf{J}_1^{-1}$ of the jacobian matrix shows the velocity ratio from the operational space to the joint space, $\mathbf{v}$ is the linear velocity of the operational space described in the tool frame $o_5x_5y_5z_5$, $\mathbf{w}$ is the angular velocity of the operational space described in the tool frame $o_5x_5y_5z_5$, $\mathbf{q}$ is the velocity of the joint space described in the corresponding joint coordinate system, and their relationship can be expressed in the following equation,

$$ \begin{bmatrix} \mathbf{v} \\ \mathbf{w} \end{bmatrix} = \mathbf{J}_1^{-1}\mathbf{q} \tag{18} $$

when $\mathbf{v} = \left(v_{x5},\ v_{y5},\ v_{z5}\right)^{\mathrm{T}}$, $\mathbf{w} = \left(w_{x5},\ w_{y5},\ w_{z5}\right)^{\mathrm{T}}$ $\mathbf{q} = \left(w_0,\ w_1,\ v_2,\ v_3,\ v_4,\ w_5\right)^{\mathrm{T}}$, and the superscript T represents the transpose of this matrix, so the following equation can be gotten by using the equation (18),

$$ \begin{bmatrix} w_0 \\ w_1 \\ v_2 \\ v_3 \\ v_4 \\ w_5 \end{bmatrix} = \left[\begin{array}{cccccc} 0 & 0 & 0 & 0 & 1 & 0 \\ 0 & 0 & 0 & -1 & 0 & 0 \\ 0 & 0 & 1 & -\frac{\sqrt{2}}{2}a_5 - d_4 & 0 & 0 \\ -1 & 0 & 0 & 0 & 0 & 0 \\ 0 & 1 & 0 & 0 & 0 & 0 \\ 0 & 0 & 0 & 0 & 0 & 1 \end{array}\right] \begin{bmatrix} v_{x5} \\ v_{y5} \\ v_{z5} \\ w_{x5} \\ w_{y5} \\ w_{z5} \end{bmatrix} \tag{19} $$

Where v_{x5} is the linear velocity of endpoint of the contact tube along x_5 axis in Fig. 8, v_{y5} is the linear velocity of endpoint of the contact tube along y_5 axis, v_{z5} is the linear velocity of endpoint of the contact tube along z_5 axis, w_{x5} is the angular velocity of the tool frame $o_5x_5y_5z_5$ around x_5 axis, w_{y5} is the angular velocity of the tool frame $o_5x_5y_5z_5$ around y_5 axis, w_{z5} is the angular velocity of the tool frame $o_5x_5y_5z_5$ around z_5 axis. v_{x5}, v_{y5}, v_{z5}, w_{x5}, w_{y5} and w_{z5} are some variables of the operational space described by

the tool frame $o_5x_5y_5z_5$. w_0 is the angular velocity of the robot around y_5 axis, because this rotational joint does not exist in the robot, so $w_0 = 0$. Increasing this joint makes that the jacobian matrix $\mathbf{J}_1$ is a square matrix, so the inverse of the jacobian matrix exists. w_1 is the angular velocity of the rotational joint 1 around z_0 axis, v_2 is the linear velocity of the translational joint 2 along z_1 axis. v_3 is the linear velocity of the translational joint 3 along z_2 axis, and it is also the speed of the vertical slider. v_4 is the linear velocity of the translational joint 4 along z_3 axis, and it is also the speed of the horizontal slider. w_5 is the angular velocity of the rotational joint 5 around z_4 axis, and the inclination angle α of the arc welding gun in the vertical plane is $45°$ during the flat welding process, so $w_5 = 0$. w_0, w_1, v_2, v_3, v_4 and w_5 are some variables of the joint space described by the corresponding joint coordinate system. The meanings of other physical quantities are the same as those in Equation (15).

Equation (19) can be changed into the following form,

$$\begin{cases} v_2 = v_{z5} - (\dfrac{\sqrt{2}}{2}a_5 + d_4)w_{x5} \\ v_3 = -v_{x5},\ v_4 = v_{y5} \\ w_0 = w_{y5},\ w_1 = -w_{x5},\ w_5 = w_{z5} \end{cases} \tag{20}$$

The meanings of the physical quantities are the same as those in Equation (19).

5.4 Trajectory planning of the welding robot

(1) linear motion

When the robot is the translational motion, the speed of the left wheel is equal to the speed of the right wheel, so the trajectory of endpoint of the contact tube is a line, and the welding speed of endpoint of the contact tube is v along the positive direction of z_5 axis in Fig. 8. According to Equation (20), the speeds of the joint space can be shown in the following equation,

$$\begin{cases} v_2 = v_{z5} = v,\ \ v_3 = v_4 = 0 \text{ m/s} \\ w_0 = w_1 = w_5 = 0 \text{ rad/s} \end{cases} \tag{21}$$

The meanings of the physical quantities are the same as those in Equation (20).

(2) Circular arc motion

When the robot rotates, the speed of the left wheel is not equal to the speed of the right wheel, so the trajectory of endpoint of the contact tube is a circular arc. At this time, the welding speed of endpoint of the contact tube is v along the positive direction of z_5 axis in Fig. 8, and $v_{z5} = v$. The angular velocity of the tool frame $o_5x_5y_5z_5$ around x_5 axis is w in Fig. 8, and $w_{x5} = w$. When $w > 0$, the welding robot rotates clockwise in Fig. 7; When $w < 0$, the welding robot rotates counterclockwise in Fig. 6. According to Equation (20), the speeds of the joint space can be shown in the following equation,

$$\begin{cases} v_2 = v_{z5} = v,\ \ v_3 = v_4 = 0 \text{ m/s} \\ w_1 = w_{x5} = w,\ \ w_0 = w_1 = w_5 = 0 \text{ rad/s} \end{cases} \tag{22}$$

The meanings of the physical quantities are the same as those in Equation (20).

6 Realization of linear fillet weld tracking

As shown in Fig. 4, the space posture $\mathbf{P}$ of the arc welding gun has been identified by using the rotating the arc sensor, and $\mathbf{P} = (l, e, \alpha, \theta)$. As shown in Fig. 2, extension or indentation of the horizontal slider can be identified by using the photoelectric position sensor and the movement speed of the horizontal slider. In order to eliminate the horizontal deviation in Fig. 8, the linear velocity v_{y5} of endpoint of the contact tube can be computed,

$$v_{y5} = \frac{e}{t_1} \tag{23}$$

Where v_{y5} is the linear velocity of endpoint of the contact tube along y_5 axis in Fig. 8. When $v_{y5} > 0$, the direction of the linear velocity v_{y5} is the positive direction of y_5 axis; When $v_{y5} < 0$, the direction of the linear velocity v_{y5} is the negative direction of y_5 axis. e is the horizontal deviation of the arc welding gun, and it can be computed by Equation (1). When $e > 0$, the arc welding gun deviates from fillet weld to the right along the welding direction. When $e < 0$, the arc welding gun deviates from fillet weld to the left along the welding direction. t_1 is the setting time used to eliminate the horizontal deviation.

In order to eliminate the height deviation in Fig. 8, the linear velocity v_{x5} of endpoint of the contact tube can be computed,

$$v_{x5} = \frac{l\cos 45° - h_0}{t_2} \tag{24}$$

Where v_{x5} is the linear velocity of endpoint of the contact tube along x_5 axis in Fig. 8. When $v_{x5} > 0$, the direction of the linear velocity v_{y5} is the positive direction of x_5 axis; When $v_{x5} < 0$, the direction of the

linear velocity v_{y5} is the negative direction of x_5 axis. l is the equivalent wire extension, h_0 is the target height that endpoint of the contact tube is relative to fillet weld, and t_2 is the setting time used to eliminate the height deviation.

Based on Equation (20) and v_{y5} in Equation (23), the speed v_4 of the horizontal slider can be calculated, and the moving distance Δd of the horizontal slider can be computed by the following equation,

$$\Delta d = \sum_{i=1}^{n} v_{4i} \Delta t_1 \tag{25}$$

Where Δd is the moving distance of the horizontal slider, v_{4i} is the speed v_4 of the horizontal slider in the i^{th} control cycle, Δt_1 is the setting time of each control cycle, and n is the total number of control cycles.

Based on Equation (20) and v_{x5} in Equation (24), the speed v_3 of the vertical slider can be calculated, and the moving distance of the vertical slider can be computed.

Movements of the vertical and horizontal sliders are not affected by the position of the horizontal slider and the output of the photoelectric position sensor, and movements of the sliders can guarantee the tracking accuracy of the welding seam.

In Fig. 8, the rotational joint around y_5 axis does not exist in the robot, so $w_{y5} = 0$. The inclination angle α of the arc welding gun in the vertical plane is $45°$ during the flat welding process, so the angular velocity of the rotational joint 5 around z_5 axis is 0, and $w_{z5} = 0$.

According to the position of the horizontal slider identified by the photoelectric position sensor, the target inclination angle θ of the arc welding gun along the welding direction divided into three situations in Fig. 9.

Classification of the target inclination angle can be expressed in the following equation,

$$\theta_{\text{target}} = \begin{cases} -2° & \text{if } \Delta d < 0 \\ 0° & \text{if } \Delta d = 0 \\ 2° & \text{if } \Delta d > 0 \end{cases} \tag{26}$$

Where θ_{target} is the target inclination angle of the arc welding gun along the welding direction. Δd is the moving distance of the horizontal slider, and it can be computed by Equation (25). If $\Delta d < 0$, the horizontal slider indents; If $\Delta d > 0$, the horizontal slider extends; If $\Delta d = 0$, the horizontal slider is in the initial position.

The rotation angle $\Delta\theta$ of the welding robot can be shown as follow,

$$\Delta\theta = \theta_{\text{target}} - \theta \tag{27}$$

Where $\Delta\theta$ is the rotation angle of the welding robot. When $\Delta\theta > 0°$, the welding robot rotates counterclockwise; When $\Delta\theta < 0°$, the welding robot rotates clockwise. θ_{target} is the target inclination angle, θ is the current inclination angle.

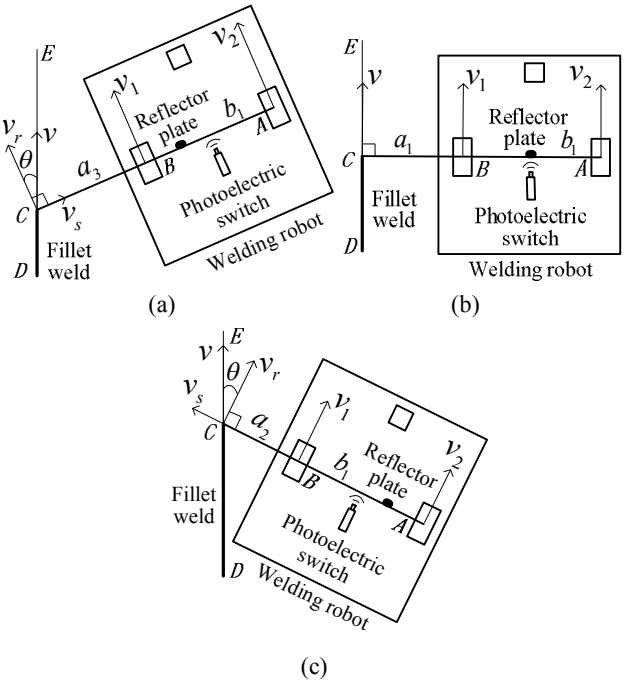

Fig. 9 Identifying the target inclination angle according to the position of the horizontal slider. (a) the target inclination angle is $2°$; (b) the target inclination angle is $0°$; (c) the target inclination angle is $-2°$

When the horizontal slider has extended, the robot rotates by using the path planning in Section 5.4, and the target inclination angle is $2°$ shown in Fig. 9(a); When the horizontal slider has indented, the robot rotates by using the path planning in Section 5.4, and the target inclination angle is $-2°$ shown in Fig. 9(c). If the current inclination angle is equal to the target inclination angle, the robot is the translational motion, and the speed of the left wheel is equal to the speed of the right wheel. At this time, the robot tracks fillet weld based on the movement of the horizontal slider, and the horizontal slider goes back to the initial position after several seconds. During the process of rotation of the robot, the horizontal slider may also return to the initial position. If the horizontal slider returns to the initial position during the welding seam tracking process, the robot rotates until the current inclination angle is equal to the target inclination angle in Fig. 9(b), then the robot is the translational motion, and a new inclination angle can be identified shown in Fig. 5. By using this algorithm, the horizontal slider is always near the initial position during the welding seam tracking process, so the length of the horizontal slider is approximate to a constant, and this is conducive to the trajectory planning of the right-angle fillet weld tracking. In order to avoid repetition, the trajectory planning of the right-angle fillet weld tracking can refer to Reference [20]. When the robot is the translational motion, the linear velocity v_{z5} of endpoint of the contact tube along z_5 axis and the angular velocity w_{x5} of the tool frame $o_5x_5y_5z_5$ around x_5 axis can be computed by Equation (21); When the robot rotates in order to adjust

the inclination angle of the arc welding gun along the welding direction, the linear velocity v_{z5} of endpoint of the contact tube along z_5 axis and the angular velocity w_{x5} of the tool frame $o_5x_5y_5z_5$ around x_5 axis can be computed by Equation (22), and experimental results show that the robot moves smoothly if w_{x5} is 0.152 rad/s.

By the front analysis, the linear velocity $\mathbf{v}$ of the operational space described in the tool frame $o_5x_5y_5z_5$ can be computed, and $\mathbf{v}=\left(v_{x5},\ v_{y5},\ v_{z5}\right)^{\mathrm{T}}$. The angular velocity $\mathbf{w}$ of the operational space described in the tool frame $o_5x_5y_5z_5$ can be computed, and $\mathbf{w}=\left(w_{x5},\ w_{y5},\ w_{z5}\right)^{\mathrm{T}}$. The linear velocity $\mathbf{v}$ and the angular velocity $\mathbf{w}$ are substituted into Equation (20), and every joint speed of the robot can be computed, so the linear fillet weld tracking has been realized.

7 Implementation of the rectangular fillet weld tracking

Fig. 10 shows the implementation of the rectangular fillet weld tracking, s_0 is the turning radius of the robot, and v is the welding speed. By using the tracking algorithm of the linear fillet weld in this paper, four linear fillet welds of the rectangular fillet weld can be tracked, and four linear fillet welds correspond to the line segment *IJ*, *LM*, *PC* and *EF*. By using the tracking algorithm of the right-angle fillet weld in Reference [20], four right-angle fillet welds of the rectangular fillet weld can be tracked, and four right-angle fillet welds correspond to the right-angle *JKL*, *MNP*, *CDE* and *FHI*. Finally, the rectangular fillet weld *DHKN* can be tracked and welded by the robot.

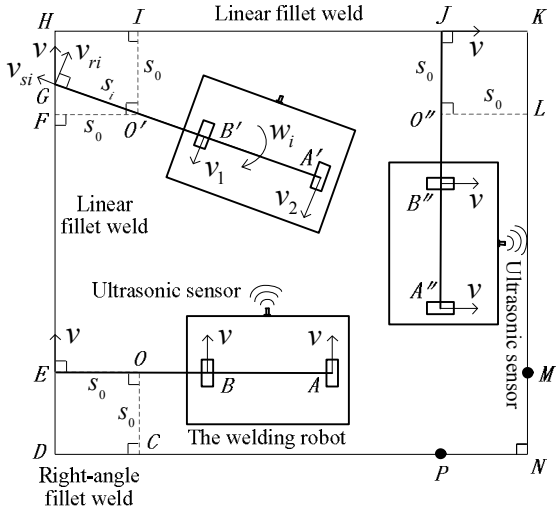

Fig. 10 Implementation of the rectangular fillet weld tracking

Fig. 11 shows the flow chart of the tracking program of the rectangular fillet weld. When the start button is pressed, the tracking program starts running.

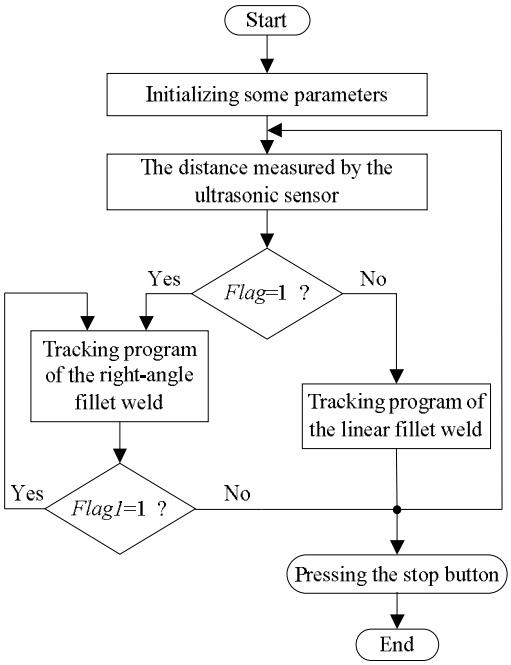

Fig. 11 The flow chart of the tracking program of the rectangular fillet weld

Firstly, some parameters should be initialized. When the distance measured by the ultrasonic sensor is not equal to the setting value of right-angle turn of the robot, the value of the variable *Flag* is set to 0, and the robot tracks the linear fillet weld by using the tracking algorithm of the linear fillet weld in this paper; When the distance measured by the ultrasonic sensor is equal to the setting value of right-angle turn of the robot, the value of the variable *Flag* is set to 1, and the robot tracks the right-angle fillet weld by using the tracking algorithm of the right-angle fillet weld in Reference [20]. When the current right-angle fillet weld welding has not been finished, the value of the variable *Flag1* is set to 1, and the robot tracks the right-angle fillet weld; When the current right-angle fillet weld welding has been finished, the value of the variable *Flag1* is set to 0, and the tracking algorithm of the right-angle fillet weld or the linear fillet weld can be chosen to run according to the output value of the ultrasonic sensor, so the program will be run circularly. When the rectangular fillet weld welding has been finished, the robot stops welding by pressing the stop button.

8 Analysis of experimental results

Welding conditions were shown as follows: Welding voltage was 25 V, and welding current was 210 A; Flux-cored wire was used, and its diameter was 1.2 mm; Mixed gas welding was used, and mixed gas consisted of 80% Ar + 20% CO_2; Low carbon steel was the parent material, and its thickness was 5 mm; Welding speed was 25 cm/min.

Fig. 12 showed that the robot welded the rectangular fillet weld, and Fig. 12(a) showed that the robot was welding the linear fillet weld. Fig. 12(b) showed the posture of the robot after welding, the inclination angle of the arc welding gun along the welding direction was within $\pm 4°$, and the position of the horizontal slider was near the initial position.

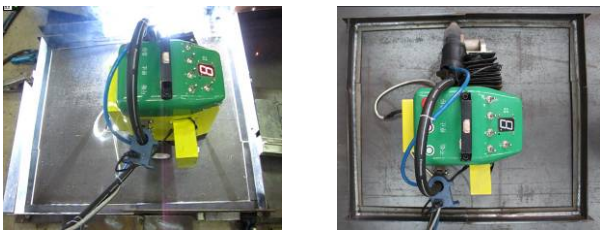

(a) (b)

Fig. 12 The robot welded the rectangular fillet weld. (a) the robot was welding the linear fillet weld; (b) the posture of the robot after welding

Fig. 13 showed the rectangular fillet weld after welding by using the design algorithm. The lengths of four sides of the rectangular fillet weld(Fig. 13a) were 74.8 cm, 62.4 cm, 74.5 cm and 62.5 cm respectively, and it is approximate to a rectangle. The rectangular fillet weld consisted of four right-angle fillet welds (Fig. 13c, e, g, i) and four linear fillet welds (Fig. 13b, d, f, h), and the magnification factor in Fig. 13(b-h) was the same as in Fig. 13(i). As shown in Fig. 13(a), four linear fillet welds were space curved welding seam actually. Because of the assembly error, the angle of the right-angle fillet weld was not 90°, but varied between 80° and 100°. It can be seen that the weld bead was smooth and the tracking precision was high from the rectangular fillet weld in Fig. 13(a-i). The experimental results showed that the robot could track the rectangular fillet weld with high accuracy.

Fig. 14 showed the error curve of the wire extension and the displacement curve of the vertical slider, Fig. 14(a) showed the error curve of the wire extension, and Fig. 14(b) showed the displacement curve of the vertical slider. When the robot tracked five linear fillet welds from the begin point to point d, point e to point j, point k to point n, point o to point q and point r to the end point, the errors of the wire extension were within ±5 mm, and the displacement of the vertical slider fluctuated within a small range. Because of the length of the right-angle fillet weld was short, the errors of the wire extension were approximate to 0 mm, so the changed displacement of the vertical slider was regarded as 0 mm when the robot tracked four right-angle fillet welds from point d to point e, point j to point k, point n to point o and point q to point r.

Fig. 15 showed the curve of the horizontal error and the displacement curve of the horizontal slider. Fig. 15(a) showed the curve of the horizontal error, and the horizontal errors were within ±0.5 mm, so the robot tracked fillet weld with high accuracy and good reliability. Fig. 15(b) showed the displacement curve of the horizontal slider. When the robot tracked five linear fillet welds from the begin point to point d, point e to point j, point k to point n, point o to point q and point r to the end point, the displacement of the horizontal slider fluctuated within a small range. When the robot tracked four right-angle fillet welds from point d to point e, point j to point k, point n to point o and point q to point r, the displacement of the horizontal slider turned bigger, then smaller. When the robot was welding the intersection point u_1, u_2, u_3 and u_4 of the right-angle weld in Fig. 15(b), the displacement of the horizontal slider was the largest, and the displacements of the horizontal slider were 82.5 mm、72.2 mm、73.2 mm and 79 mm respectively. The largest displacements were different, and the reason were shown as follows: at the beginning of the right-angle turn of the robot, the positions of the horizontal slider were different, the inclination angles of the arc welding gun along the welding direction were different, and the actual angles of the right-angle fillet welds were different.

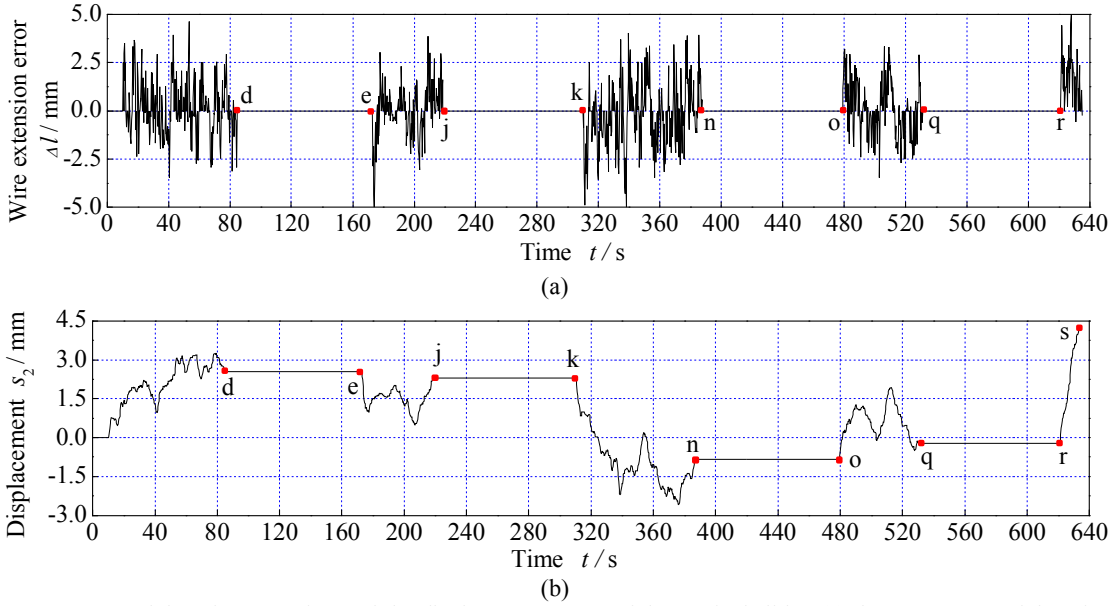

Fig. 14 The error curve of the wire extension and the displacement curve of the vertical slider. (a) the error curve of the wire extension; (b) the displacement curve of the vertical slider

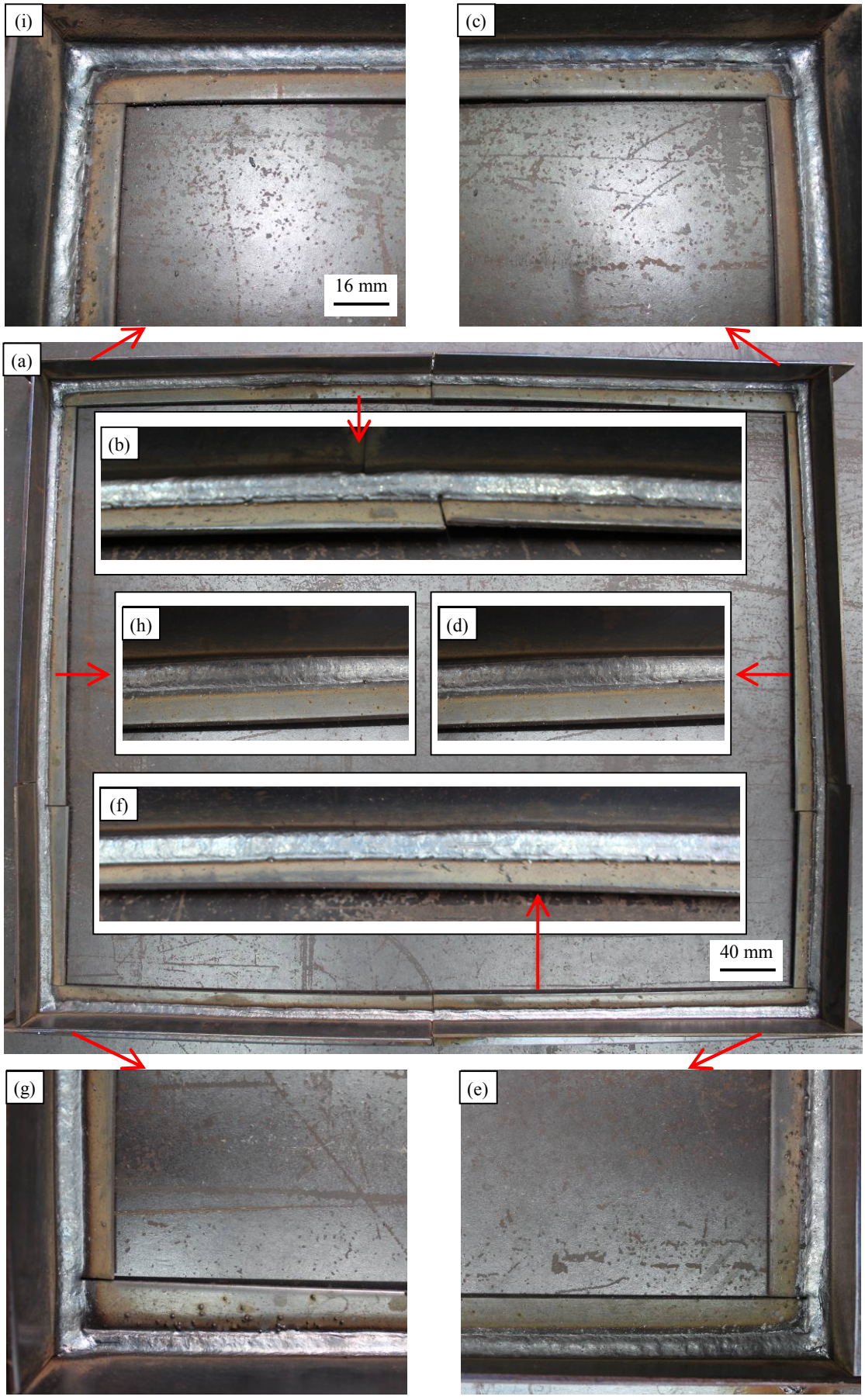

Fig. 13 Rectangular fillet weld welding experiments. (a) rectangular fillet weld after welding; (b) the first linear fillet weld after welding; (c) the first right-angle fillet weld after welding; (d) the second linear fillet weld after welding; (e) the second right-angle fillet weld after welding; (f) the third linear fillet weld after welding; (g) the third right-angle fillet weld after welding; (h) the fourth linear fillet weld after welding; (i) the fourth right-angle fillet weld after welding

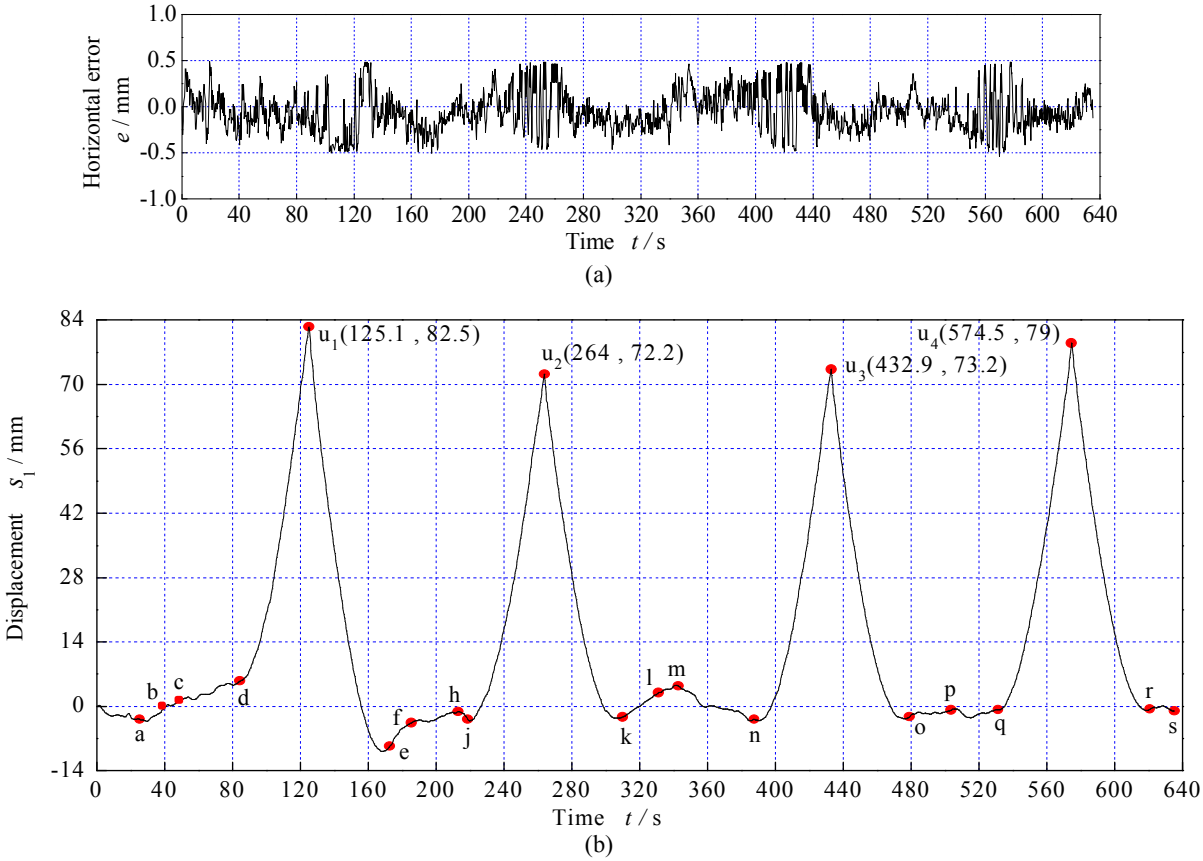

Fig. 15 The curve of the horizontal error and the displacement curve of the horizontal slider. (a) the curve of the horizontal error; (b) the displacement curve of the horizontal slider

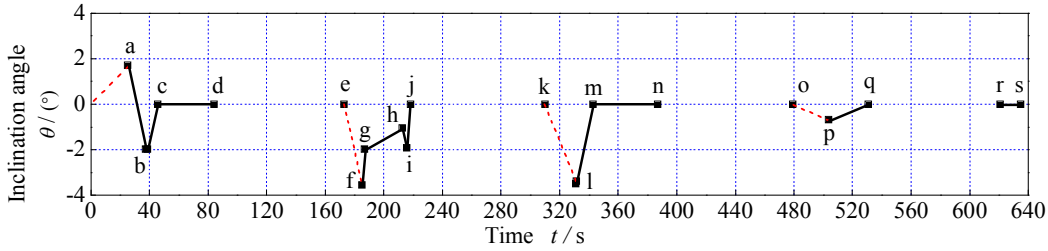

Fig. 16 The inclination angle curve of the arc welding gun along the welding direction when the robot tracked the linear fillet weld

Fig. 16 showed that the curve of the inclination angle of the arc welding gun along the welding direction when the robot tracked the linear fillet weld, and the dotted line showed the process of measuring the inclination angle. The inclination angle was regarded as $0°$ at the end of the right-angle fillet weld. By using the algorithm in Fig. 5, the inclination angle could be identified during the tracking process of the linear fillet weld. Because the wheels of the robot skidded during the welding process, the inclination angle would change. By using design algorithm, the inclination angle of the arc welding gun along the welding direction was within $\pm 4°$ in Fig. 16. At the endpoint, the displacement curve of the horizontal slider was -1.06 mm, and the inclination angle was approximate to $0°$, so the experimental results showed the correctness of the design algorithm.

Fig. 17 showed the contrast figures of the linear fillet weld after the manual welding and the robotic welding in the factory, and Fig. 17(a) showed that some workers were welding. Strong arc light and a lot of toxic smoke were generated during the welding process, which was bad for worker's health. Fig. 17(b) showed that the robot was welding, and the welding quality was not affected by bad environment.

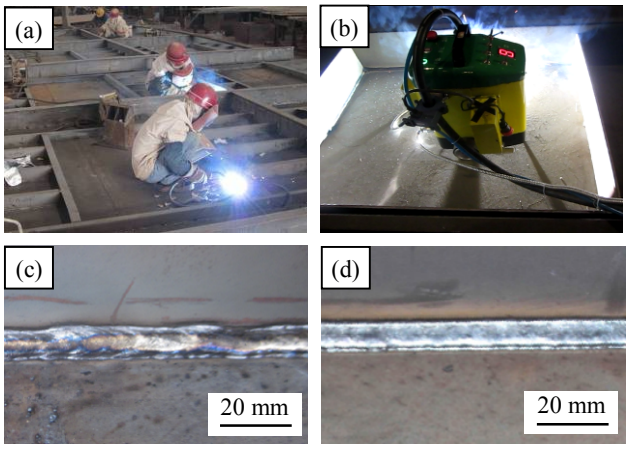

Fig. 17 The contrast figures of the linear fillet weld after the manual welding and the robotic welding in the factory. (a) Workers were welding the rectangular fillet weld; (b) The welding robot was welding the rectangular fillet weld; (c) the welding seam after the manual welding; (d) the linear fillet weld after the robotic welding

Fig. 17(d) showed the welding seam after the robotic

welding, and the measuring results showed that the size of the vertical weld leg was approximately equal to the size of the horizontal weld leg, so the horizontal deviations that the arc welding gun deviated from fillet weld were small. By using the welding robot, the welding speed was approximately a constant, and it could be controlled by manipulating the human-computer interface, so the weld bead was more uniform and smooth than that welded by the manual welding in Fig. 17(c). By using the designed algorithm, the welding robot could tracked the rectangular fillet weld with high accuracy and good reliability.

Fig. 18 showed the calculation method of the deviation that the arc welding gun deviated from fillet weld, and the area in the curve *BDEB* is the cross section of weld bead. Line segment *BD* is the vertical weld leg, line segment *DE* is the horizontal weld leg, and point *G* is the midpoint of the line segment *BE*.

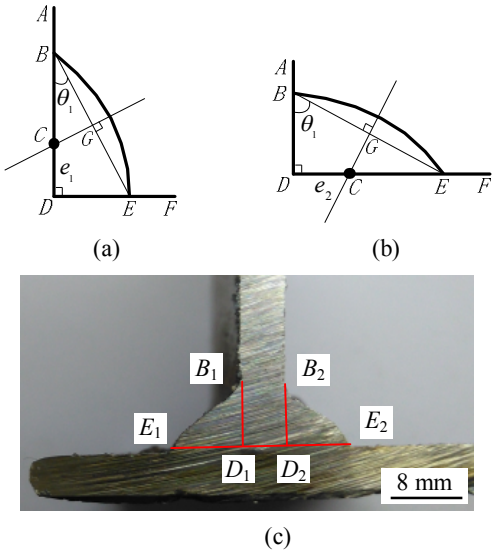

Fig. 18 The calculation method of the deviation that the arc welding gun deviated from fillet weld. (a) the horizontal weld leg $|DE| \le$ the vertical weld leg $|BD|$; (b) the horizontal weld leg $|DE| >$ the vertical weld leg $|BD|$; (c) the real figure of the cross section of weld bead

(a) The size of the horizontal weld leg $DE \le$ the size of the vertical weld leg BD

As shown in Fig. 18(a), the size of the vertical weld leg is greater than the size of the horizontal weld leg, and point *C* is the intersection point between the perpendicular bisector of the line segment *BE* and the vertical weld leg *BD*. The length of the line segment *CD* is equal to the deviation e_1 that the arc welding gun deviates from fillet weld upward, and the geometric relationship can be shown in the following equation,

$$\cos\theta_1 = \frac{|BD|}{|BE|} = \frac{|BG|}{|BC|} \tag{28}$$

the length of the line segment *BC* can be calculated by using the equation (28),

$$|BC| = \frac{|BE||BG|}{|BD|} = \frac{|BD|^2 + |DE|^2}{2|BD|} \tag{29}$$

The deviation e_1 can be calculated by using the equation (29),

$$e_1 = |CD| = |BD| - |BC| = \frac{|BD|^2 - |DE|^2}{2|BD|} \tag{30}$$

In the equations (28-30), θ_1 is the size of $\angle DBE$, $|BD|$ is the length of the line segment *BD*, $|BE|$ is the length of the line segment *BE*, $|BG|$ is the length of the line segment *BG*, $|BC|$ is the length of the line segment *BC*, and $|DE|$ is the length of the line segment *DE*. e_1 is the deviation that the arc welding gun deviates from fillet weld upward, and its value is equal to the length of the line segment *CD* in Fig. 18(a).

(b) The size of the horizontal weld leg $DE >$ the size of the vertical weld leg BD

As shown in Fig. 18(b), the size of the vertical weld leg is smaller than the size of the horizontal weld leg, and point *C* is the intersection point between the perpendicular bisector of the line segment *BE* and the horizontal weld leg *DE*. The length of the line segment *CD* is equal to the deviation e_2 that the arc welding gun deviates from fillet weld to the right, and the geometric relationship can be shown in the following equation,

$$\sin\theta_1 = \frac{|DE|}{|BE|} = \frac{|GE|}{|CE|} \tag{31}$$

the length of the line segment *CE* can be calculated by using the equation (31),

$$|CE| = \frac{|BE||GE|}{|DE|} = \frac{|BD|^2 + |DE|^2}{2|DE|} \tag{32}$$

The deviation e_2 can be calculated by using the equation (32),

$$e_2 = |CD| = |DE| - |CE| = \frac{|DE|^2 - |BD|^2}{2|DE|} \tag{33}$$

In the equations (31-33), e_2 is the deviation that the arc welding gun deviates from fillet weld to the right, and its value is equal to the length of the line segment *CD* in Fig. 18(b). In addition, the meanings of the other physical quantities are the same as those in the equations (28-30).

Fig. 18(c) is the real figure of the cross section of weld bead. Along the perpendicular direction of fillet weld, the steel sample after welding was cut, and the cross section of weld bead was gotten. After measuring, it could be found that the size of the vertical weld leg B_1D_1 of the left weld bead was 7.8 mm, and the size of the horizontal weld leg D_1E_1 of the left weld bead was 8 mm. Because the size of the horizontal weld leg was greater than the size of the vertical weld leg, the deviation that the arc welding gun deviated from fillet weld to the left was 0.198 mm by using the equation (33). Similarly, the size of the vertical weld leg B_2D_2 of the right weld bead was 7.5 mm, and the size of the horizontal weld leg D_2E_2 of the right weld bead was 7.6 mm. Because the size of the horizontal weld leg was greater than the size of the vertical weld leg, the deviation that the arc welding gun

deviated from fillet weld to the right was 0.099 mm by using the equation (33).

Based on the coordinated movement among two wheels, the horizontal slider and the vertical slider, the robot can track the rectangular fillet weld that is curved in the height and horizontal directions, and appearance of fillet weld after welding is well. After welding, the horizontal slider returns to the initial position, and the inclination angle of the arc welding gun along the welding direction is approximate to $0°$. The posture of the robot after welding is approximate to the posture of the robot at the beginning of welding, which illustrates the correctness of the design algorithm.

9 Conclusion

(1) The structure of the robot and the whole system of tracking and welding have been introduced, and the working principle of the rotating arc sensor has been studied. The mathematical model of the space posture of the arc welding gun has been established, and the mathematical model $\mathbf{P}$ can be expressed as $\mathbf{P}=(l,e,\alpha,\theta)$. l is the equivalent wire extension, e is the horizontal deviation, α is the inclination angle of the arc welding gun in the vertical plane, and θ is the inclination angle of the arc welding gun along the welding direction.

(2) The equivalent link coordinate systems of the wheeled mobile robot have been built, and the jacobian matrix of the robot and its inverse matrix have been calculated. The transformation from the operational space speed to the joint space speed has been realized by using the inverse matrix of the jacobian matrix, and the trajectory planning of the welding robot has been finished.

(3) The tracking algorithms of the linear fillet weld and the rectangular fillet weld have been studied, and the tracking experiments of the rectangular fillet weld have been done in the laboratory and the factory. The curves of the wire extension error, the horizontal error and the inclination angle have been studied during the welding process of the rectangular fillet weld. After welding, the horizontal slider returns to the initial position, and the inclination angle of the arc welding gun along the welding direction is approximate to $0°$. Four right-angle fillet welds and four linear fillet welds were tracked with high accuracy, and experiment results showed that the robot could track the rectangular fillet weld with high accuracy and good reliability.

Acknowledgments The work is supported by the National High Technology Research and Development Program of China (863 Program), No. 2013AA041003, the Innovation Fund Designated for Graduate Students of Jiangxi Province, China, No. YC2016-B009, and the Nanchang University PhD Student Abroad Visiting Plan in 2016. The authors thank the reviewers for their valuable comments and suggestions.

References

1. Ku N, Cha JH, Lee KY, Kim J, Kim TW, Ha S, Lee D (2010) Development of a mobile welding robot for double-hull structures in shipbuilding. Journal of Marine Science and Technology 15(4): 374-385
2. Liu SY, Wang GR, Zhang H, Jia JP (2010) Design of robot welding seam tracking system with structured light vision. Chinese Journal of Mechanical Engineering 23(4): 436-442
3. Nele L, Sarno E, Keshari A (2013) An image acquisition system for real-time seam tracking. International Journal of Advanced Manufacturing Technology 69(9): 2099-2110
4. Gu WP, Xiong ZY, Wan W (2013) Autonomous seam acquisition and tracking system for multi-pass welding based on vision sensor. International Journal of Advanced Manufacturing Technology 69(1): 451-460
5. Xu YL, Fang G, Lv N, Chen SB, Zou JJ (2015) Computer vision technology for seam tracking in robotic GTAW and GMAW. Robotics and Computer-Integrated Manufacturing 32(2): 25-36
6. Chen B, Feng JC (2014) Modeling of underwater wet welding process based on visual and arc sensor. Industrial Robot-An International Journal 41(3): 311-317
7. Xu YL, Yu HW, Zhong JY, Lin T, Chen SB (2012) Real-time seam tracking control technology during welding robot GTAW process based on passive vision sensor. Journal of Materials Processing Technology 212(8): 1654-1662
8. Shen HY, Lin T, Chen SB, Li LP (2010) Real-time seam tracking technology of welding robot with visual sensing. Journal of Intelligent & Robotic Systems 59(3): 283-298
9. Xu YL, Lv N, Zhong JY, Chen HB, Chen SB (2012) Research on the real-time tracking information of three-dimension welding seam in robotic GTAW process based on composite sensor technology. Journal of Intelligent & Robotic Systems 68(2): 89-103
10. Wang XW (2014) Three-dimensional vision-based sensing of GTAW a review. International Journal of Advanced Manufacturing Technology 72(1): 333-345
11. Kim CH, Na SJ (2001) A study of an arc sensor model for gas metal arc welding with rotating arc-Part 1: dynamic simulation of wire melting. Proceedings of the Institution of Mechanical Engineers Part B-Journal of Engineering Manufacture 215(9): 1271-1279
12. Kim CH, Na SJ (2001) A study of an arc sensor model for gas metal arc welding with rotating arc-Part 2: simulation of an arc sensor in mechanically rotating gas metal arc welding. Proceedings of the Institution of Mechanical Engineers Part B-Journal of Engineering Manufacture 215(9): 1281-1288
13. Lee GY, Oh MS, Kim SB (2003) Development of a high speed rotating arc sensor system for tracking complicate curved fillet welding lines. International Journal of Precision Engineering and Manufacturing 4(6): 6-14
14. Kim Y, Rhee S (2005) Arc sensor model using multiple-regression analysis and a neural network. Proceedings of the Institution of Mechanical Engineers Part B-Journal of Engineering Manufacture 219(6): 431-446
15. Yoo WS, Shi YH, Kim JT, Na SJ (2006) End point detection of fillet weld using mechanized rotating arc sensor in GMAW. Welding Journal 85(8): 180S-187S
16. Shi YH, Yoo WS, Na SJ (2006) Mathematical modelling of rotational arc sensor in GMAW and its applications to seam tracking and endpoint detection. Science and Technology of Welding and Joining 11(6): 723-730
17 Xu YL, Zhong JY, Ding MY, Chen HB, Chen SB (2013) The acquisition and processing of real-time information for height tracking of robotic GTAW process by arc sensor. International Journal of Advanced Manufacturing Technology 65(5): 1031-1043.
18. Le J, Zhang H, Xiao Y (2017) Circular fillet weld tracking in GMAW by robots based on rotating arc sensors. International Journal of Advanced Manufacturing Technology 88(9): 2705-2715
19. Cai ZX (2009) Robotics. Tsinghua university press.
20. Le J, Zhang H, Chen XQ (2017) Right-angle fillet weld tracking by robots based on rotating arc sensor in GMAW. International Journal of Advanced Manufacturing Technology, 10.1007/s00170-017-0536-2